American Journal of Physical Chemistry
2022; 11(4): 110-119
http://www.sciencepublishinggroup.com/j/ajpc
doi: 10.11648/j.ajpc.20221104.14
ISSN: 2327-2430 (Print); ISSN: 2327-2449 (Online)

Green Synthesis of Iron Oxide Nanoparticles Using Grapefruit Peel Extract: Application for Removal of Indigo Carmine Dye from Industrial Wastewater

N'guessan Louis Berenger Kouassi[1, *], Donourou Diabate[2], Lemeyonouin Aliou Guillaume Pohan[1], Benjamin Diby Ossonon[1], Luc Dou Blonde[2], Albert Trokourey[2]

[1]Training Research Unit of Biological Sciences, Department of Mathematic Physic and Chemical, University of Peleforo Gon Coulibaly, Korhogo, Côte d'Ivoire

[2]Laboratory of Constitution and Reaction of Matter, University of Felix Houphouet Boigny, Abidjan, Côte d'Ivoire

Email address:

kberenger2015@gmail.com (N'guessan Louis Berenger Kouassi)

[*]Corresponding author

To cite this article:

N'guessan Louis Berenger Kouassi, Donourou Diabate, Lemeyonouin Aliou Guillaume Pohan, Benjamin Diby Ossonon, Luc Dou Blonde, Albert Trokourey. Green Synthesis of Iron Oxide Nanoparticles Using Grapefruit Peel Extract: Application for Removal of Indigo Carmine Dye from Industrial Wastewater. *American Journal of Physical Chemistry*. Vol. 11, No. 4, 2022, pp. 110-119.
doi: 10.11648/j.ajpc.20221104.14

Received: October 15, 2022; **Accepted**: November 10, 2022; **Published**: November 29, 2022

Abstract: Synthesis of iron oxide nanoparticles by green approach is extremely promising because of its non-toxicity and environmentally friendly behavior. However, few studies have been done on the synthesis of iron oxide nanoparticles using grapefruit peel extract. The aim of the present study was to remove indigo carmine dye from industrial effluent using iron oxide nanoparticles synthesized via grapefruit peel extract. The green iron oxide nanoparticles were characterized by SEM, FTIR, and XRD techniques. The antioxidant activity of green iron oxide was also determined. Batch adsorption experiments were used to investigate the adsorption capacities of indigo carmine by iron oxide nanoparticles in synthetic solutions and industrial effluent. The results showed that the synthesized γ-Fe_2O_3 surface is coated with grapefruit peel extract. The green γ-Fe_2O_3 nanoparticles were semi-spherical with an average crystallite size of 11.9 nm, and showed antioxidant activity against DPPH. In the synthetic aqueous solution, the optimum pH value was 2.4 with an indigo carmine adsorption percentage of 84.72%. The kinetic study showed that indigo carmine adsorption by γ-Fe_2O_3 followed the second-order model and the adsorption process is governed both by external surface adsorption and intra-particle diffusion. Moreover, indigo carmine adsorption by γ-Fe_2O_3 was well fitted by the Langmuir model. The maximum adsorption percentage in an aqueous solution was 96%. The investigation with industrial effluent indicated that the adsorption percentage of indigo carmine was 28.68%. Therefore, γ-Fe_2O_3 nanoparticles from grapefruit peel extract may be proposed to purify industrial effluents contaminated by indigo carmine.

Keywords: Green Synthesis, Iron Oxide Nanoparticles, Indigo Carmine, Adsorption, Industrial Effluent

1. Introduction

During the last decades, nanoparticles have gained more interest due to their application in multiple fields such as physics, chemistry, biomedicine, optics, electronics, and catalysis [1]. These nanoparticles are commonly synthesized using various chemical and physical methods including chemical deposit in the steam phase, sol-gel transition, ablation laser, engraving, thermal decomposition, and mechanical milling [2, 3]. These physicochemical methods require the use of toxic substances and are expensive. To solve these problems, environmentally friendly alternative methods have been developed. Hence, several studies have been done on the biosynthesis of nanoparticles through green product extracts such as fruit peels [4-7]. Fruit peels are used because they contained various phytochemicals such as

flavonoids and polysaccharide compounds, and they are renewable resources. Studies on the biosynthesis of nanoparticles using fruit peels were focused on citrus maxima peels [8], citrus reticulum peels [4], avocado peels [5], pineapple peels [9, 10], banana peels [6, 7], and onion peels [11-13]. However, few studies have been done on the synthesis of iron oxide nanoparticles via grapefruit peels.

Indigo carmine dye is commonly used in many fields such as the textile, food, pharmaceutical, printing, and leather industries [14]. Water contamination by indigo carmine is a global problem due to its negative effects on human health and the aquatic environment [15]. For example, the presence of indigo carmine in the aquatic environment reduces light penetration, which negatively affects photosynthesis. Indigo carmine ingestion by Humans causes skin and eye irritations, difficulty breathing [15], and can damage the neurological system [16]. However, indigo carmine removal from wastewater is important. Thus, several methods such as filtration, electrocoagulation processes, oxidation, and adsorption have been developed to treat dyestuffs wastewater [17-21]. Among them, the adsorption technique is well used due to its low cost, easy material handling, depending on the system, and pollutants removal efficacy. Adsorbents frequently used to remove indigo carmine are activated carbon [21, 22], graphene oxide [23], and chitosan [24]. However, few studies have focused on the use of iron oxide nanoparticles (FeONPs) to treat indigo carmine-charged wastewater. The objective of this study is to investigate indigo carmine removal from textile effluent through the adsorption phenomena using green iron oxide nanoparticles (FeONPs). To achieve this, the FeONPs were synthesized and characterized. The effects of contact time, initial concentration of indigo carmine, and solution pH on the adsorption of indigo carmine in synthetic aqueous solution were studied. Finally, FeONP with industrial effluent was explored in practical application.

2. Material and Methods

2.1. Materials and Chemicals

The reagents used in this study include sodium hydroxide NaOH, chloride acid HCl, 1,1-Diphenyl-2-Picrylhydrazyl (DPPH), Ethanol, $FeSO_4{\cdot}7H_2O$, $FeCl_3{\cdot}6H_2O$, and indigo carmine ($C_{16}H_8N_2Na_2O_8S_2$). The concentrations of indigo carmine in the solutions before and after adsorption were determined using the spectrometer at 610 nm. A pH meter HANNA HI.9828 was used to measure the values of pH.

2.2. Green Synthesis of Iron Oxide Nanoparticles

The grapefruit peels were purchased from Yamoussoukro's small market, washed several times with deionized water, and dried at room temperature. The dried peels were grounded and sieved. The grapefruit peel extract was prepared according to Ruíz-Baltazar et al. [1] with slight modifications. About 20 g of yellowish peels of grapefruit were placed into a 500 mL Erlenmeyer flask containing 200 mL Milli Q water and heated at 80°C for 30 min. The obtained extract was filtered and stored at 4°C for further experimentation. The FeONPs were synthesized as follows: 6.95 g of $FeSO_4{\cdot}7H_2O$ and 13.51 g of $FeCl_3{\cdot}6H_2O$ (1/2 molar ratio) were dissolved in 250 mL of deionized water and heated at 80°C under stirring using a magnetic stirrer. After 5 minutes, 20 mL of the grapefruit peel extract solution was added to the mixture. Five minutes later, 1 M of NaOH aqueous solution was added drop-wise to the mixture until pH was between 10-11. The formation of an intense black-colored solution confirmed the synthesis of FeONPs. The products were separated from the solution and washed with Milli Q water many times. Finally, the FeONPs were dried in an oven at 80°C for 24 hours.

2.3. Characterization of Green Iron Oxide Nanoparticles

2.3.1. SEM, XRD and FTIR Analysis

The prepared green iron oxide nanoparticles were characterized by a field-emission gun source scanning electron microscope (FEG-SEM; JEOL/JEM-1230). The X-ray powder diffraction (XRD) patterns of green iron oxide nanoparticles were recorded using a diffractometer Bruker D8 Advance X-ray diffractometer θ/2θ with Cu-Kα radiation (λ = 1.542 Å). The data were collected between 5° and 90° by using 0.02° increments and an integration time of 1.3 s per increment with a scintillator detector. Fourier transform infrared (FTIR) spectroscopy was employed to characterize grapefruit peel extract and green iron oxide nanoparticles using the Nicolet 6700 FTIR in the 3800–700 cm^{-1} region.

2.3.2. Antioxidant Activity

Antioxidant capacities of green FeONPs were determined using the method described by Kumar et al. [25] with slight modifications. Various concentrations of the green FeONPs (2 mg/mL, 1 mg/mL, 0.5 mg/mL, 0.25 mg/mL, 0.125 mg/mL and 0.0625 mg/mL) were prepared using an absolute ethanol. Then, 1.0 mL of 0.3 mg/mL of DPPH solution (in 98% ethanol) was added to each green FeONPs solution. The mixture was vortexed vigorously and was incubated in the dark for 30 min at room temperature. After it, the absorbance of the reaction mixture was measured at 517 nm using a spectrophotometer JENWAY. The percentage of inhibition of free radicals was determined as follows [25]:

$$\text{Scavenging activity } (\%) = \frac{(A_0 - A_i)\times 100}{A_0} \quad (1)$$

Where A_0 is the absorbance of the control (blank) and A_i is the absorbance in the presence of the green FeONPs.

2.3.3. pH at the Point of Zero Charge (pHpzc)

The pHpzc of FeONPs was determined according to the method proposed by Kouassi et al. [26]. Various solutions of 0.01 M NaCl of pH ranging between 2 and 12 were prepared. The pH was adjusted with 0.1 M NaOH or 0.1 M HCl solution. Then, 0.1 g of FeONP was suspended in 50 mL of 0.01 M NaCl solution and agitated for 48 h [26]. After agitation and filtration, the final pH of the filtrate was measured. The curve of $(pH_{final} - pH_{initial})$ vs. $pH_{initial}$ was used to determine the

value of pHpzc which is the intercept point of the curve $(pH_{final} - pH_{initial})$vs. $pH_{initial}$ with the $pH_{initial}$ line [26].

2.3.4. Crystallite Size

The average crystallite size of green iron oxide particles was calculated using Debye Scherrer's equation [27]:

$$D(nm) = \frac{k \times \lambda}{FWHM \times \cos\theta} \quad (2)$$

Where k = 0.9 is the shape constant, λ = 1.54056 Å is the wavelength of the X-Ray used (Cu-Kα), and FWHM is the full width at half maxima of the diffraction peak at an angle 2θ.

2.4. Adsorption Study in Aqueous Solution

The adsorption tests were carried out at room temperature. To study the effect of contact time, a mass of 1 g of FeONP was placed in 200 mL of 10 mg/L of an indigo carmine solution, and the suspension was continuously agitated. At various time intervals (5 min, 10 min, 20 min, 30 min, 60 min, 120 min, 150 min, 180 min, and 240 min) 5 mL was collected. Indigo carmine isotherm experiments were investigated by varying initial concentrations from 10 to 100 mg/L. The mass of 0.3 g was added to 25 mL of indigo carmine solutions, and the suspensions were agitated for the equilibrium time. The effect of pH was carried out by setting the concentration of indigo carmine and FeONP mass at 10 mg/L and 0.1 g, respectively, and varying the pH from 2 to 10.

Equations (3) and (4) give the adsorption percentage, and the amount of indigo carmine adsorbed at time t, respectively.

$$\%\,Ads = \frac{(C_0 - C_e) \times 100}{C_0} \quad (3)$$

$$q_t = \frac{(C_0 - C_t) \times V}{m} \quad (4)$$

Where C_0 (mg/L) and Ce (mg/L) are the initial, and equilibrium of indigo carmine, respectively. Ct (mg/L) represents the indigo carmine concentration in the solution after a contact time t (min), V (L) is the volume of the solution, and m (g) is the mass of the FeONP.

At the equilibrium, the amount of indigo carmine adsorbed was calculated as follows:

$$q_e = \frac{(C_0 - C_e) \times V}{m} \quad (5)$$

Where C_0 (mg/L) and C_e (mg/L) are the initial, and equilibrium indigo carmine concentrations, respectively; V (L) is the volume of solution, and m (g) is the FeONP mass.

2.5. Adsorption Study in Industrial Effluent

The industrial effluent sample was collected around a paint manufacturing industry in Abidjan City which is the biggest town in Côte d'Ivoire. A mass of 0.1 g of FeONP was added to 20 mL of the sample containing 13.7 mg/L of indigo carmine. An aqueous solution of indigo carmine of 15 mg/L was prepared. The adsorption with both samples (wastewater and aqueous solutions) was conducted in batch tests during 2h at room temperature.

2.6. Kinetic and Isotherm Adsorption Models

2.6.1. Kinetic Models

Various kinetic models such as pseudo-first-order [28], pseudo-second-order [29], and intra-particle diffusion model [30] were used in the present study.

Equations (6) and (7) give the expressions of the nonlinear forms of the pseudo-first-order model, and the pseudo-second-order model, respectively:

$$q_t = q_e[1 - \exp(-k_1 t)] \quad (6)$$

$$q_t = \frac{q_e^2\, k_2\, t}{1 + q_e\, k_2\, t} \quad (7)$$

Where k_1 (min^{-1}) represents the rate constant of the pseudo-first-order, k_2 (g. $mg^{-1}.min^{-1}$) represents the rate constant of the pseudo-second-order model, q_t (mg/g) and q_e (mg/g) are the amounts of indigo carmine adsorbed at time t (min) and equilibrium, respectively.

Equation (8) gives the expression of the intraparticle diffusion model [30].

$$q_t = k_{id}\sqrt{t} + C \quad (8)$$

Where q_t (mg/g) is the amount of indigo carmine adsorbed at time t (min), k_{id} is the rate constant of the intraparticle diffusion model and C is the intercept.

2.6.2. Adsorption Isotherm Models

The adsorption isotherms models such as Langmuir [31], Freundlich [32], and Sips [33] models were applied in the present study.

The equations (9), (10), and (11) give the expressions of the nonlinear forms of Langmuir, Freundlich, and Sips adsorption models, respectively:

$$Q_e = \frac{Q_{max} \times K_L \times C_e}{1 + (K_L \times C_e)} \quad (9)$$

$$Q_e = K_F \times C_e^{\,1/n} \quad (10)$$

$$Q_e = \frac{Q_{ms} \times K_S \times C_e^{ms}}{1 + K_S \times C_e^{ms}} \quad (11)$$

Where C_e (mg/L) is the equilibrium indigo carmine concentration; Qe (mg/g) is the amount of indigo carmine adsorbed at equilibrium, K_L (L/mg) is the Langmuir constant, K_F is the Freundlich constant, K_S (L/mg) is the Sips constant, Q_{max} (mg/g) is the Langmuir maximum amount adsorbed, Qms (mg/g) is the Sips maximum adsorption capacity, n is the Freundlich model exponent, and ms is the Sips model exponent.

The favorability of adsorption is indicated by the Langmuir parameter (R_L) which is calculated as follows [26]:

$$R_L = \frac{1}{1 + K_L \times C_0} \quad (12)$$

Where C_0 is the highest initial solute concentration. $R_L < 1$ indicates unfavorable adsorption, the adsorption is favorable when $0 < R_L < 1$, and the adsorption is irreversible when $R_L = 0$ [26].

2.7. Error Analysis

In order to find the best nonlinear model, an error analysis was performed. For this the Sum of Squares Errors (SSE), and the Chi-square (χ^2) were achieved by the following equations [26]:

$$SSE = \sum_{i=1}^{n}(q_{e\ exp} - q_{e\ cal})^2 \quad (13)$$

$$\chi^2 = \sum_{i=1}^{n}\frac{(q_{e\ exp}-q_{e\ cal})^2}{q_{e\ cal}} \quad (14)$$

Where $q_{e\ exp}$ and $q_{e\ cal}$ are experimental and predicted adsorption capacities at equilibrium time, respectively.

3. Results and Discussion

3.1. Properties of the Green Iron Oxide Nanoparticles

3.1.1. SEM Analysis

As shown in the SEM image (Figure 1), the morphology of FeONP is semi-spherical with several agglomerates. The agglomeration observed by SEM is due to the magnetic interaction generated by individual iron oxide nanoparticle [1]. The biological compounds of the grapefruit peels present on the nanoparticles' surfaces can also explain the formation of the agglomerates. In addition, the stability of FeONP may be improved by the grapefruit peel biomolecules [2, 8].

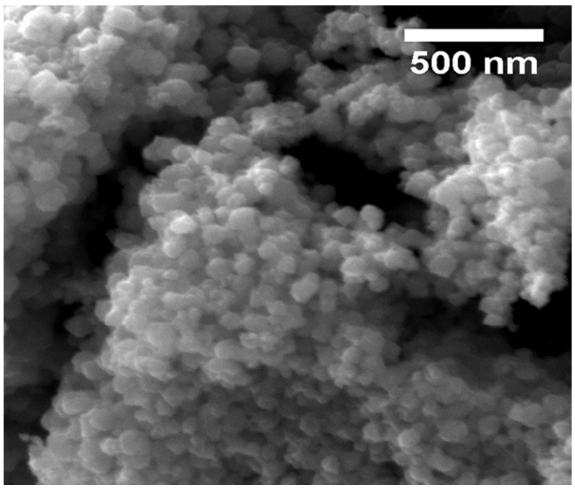

Figure 1. *SEM image of green FeONP.*

3.1.2. XRD Analysis

The XRD data of grapefruit peel extract mediated iron oxide nanoparticles are shown in Figure 2. The results showed diffraction peaks at 23.73°, 27.86°, 30.16°, 31.79°, 35.41°, 43.27°, 45.41°, 48.5°, 56.40°, 57.21°, 62.77°, 74.26°, 75.41°, and 89.9°corresponding to the indexes of (210), (211), (220), (221), (311), (400), (410), (330), (510), (511), (440), (533), (622), and (731), respectively. These crystal planes indicate the formation of maghemite (γ-Fe_2O_3) nanoparticles (JCPDS 39-1346). The results also revealed that γ-Fe_2O_3 nanoparticles formed by the reduction method using grapefruit peel extract were crystalline, as indicated by the intense peak observed at 31,79° which corresponds to the index of (221) [34]. The average crystallite size calculated using the Debye-Scherrer equation was 11.9 nm.

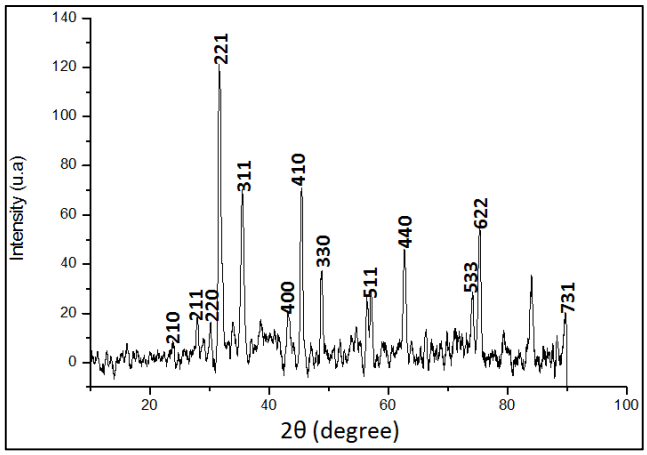

Figure 2. *XRD patterns of the green iron oxide.*

3.1.3. FITR Analysis

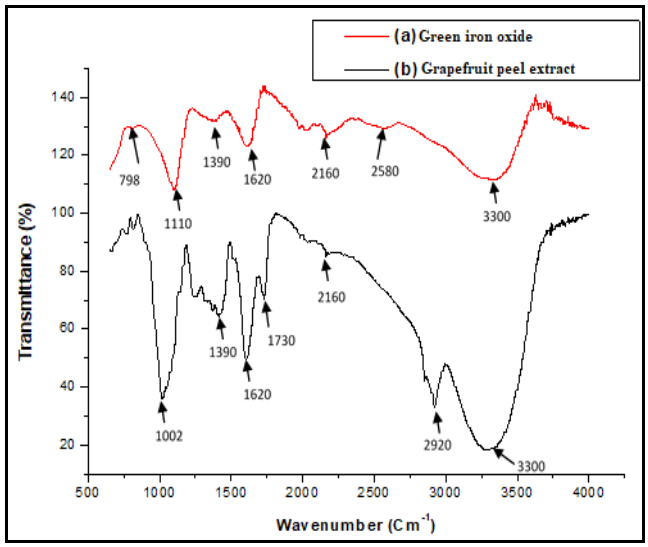

Figure 3. *FTIR spectrum of green iron oxide nanoparticle (a) and grapefruit peel extract (b).*

The FTIR results of the grapefruit peel extract and FeONP are given in Figure 3. Figure 3b showed peaks at 1002 cm^{-1}, 1390 cm^{-1}, 1620 cm^{-1}, 1730 cm^{-1}, 2160 cm^{-1}, 2920 cm^{-1} and 3300 cm^{-1}. The FTIR spectrum of green FeONP (Figure 3a) indicated some peaks at 798 cm^{-1}, 1110 cm^{-1}, 1390 cm^{-1}, 1620 cm^{-1}, 2160 cm^{-1}, 2580 cm^{-1}, and 3300 cm^{-1}. According to Kumar et al. [25], the band at 3300 cm^{-1} is attributed to phenolic O–H, or alcoholic O-H stretching of flavonoids, or organic acids, respectively. The peaks at 2920 cm^{-1} and 2580 cm^{-1} are assigned to C-H stretching vibrations in methyl or methoxy groups [25, 35]. The FITR of grapefruit peel extract indicates the presence of stretching C=O vibration of acid derivatives, which is confirmed by the peak at 1730 cm^{-1} [25]. The band observed at 1390 cm^{-1} is assigned to the aromatics compounds such as polysaccharides [1, 25]. With the grapefruit peel extract spectrum, the strong peak at 1002 cm^{-1}

is attributed to -C-O-C stretching of ether and ester groups [25]. The FTIR spectrum of FeONP showed a signal at 1620 cm^{-1} which is assigned to C=O vibration in aldehydes and ketones, indicating the presence of phenolic acid and terpenoid [25]. The band observed at 798 cm^{-1} on the spectrum of FeONP is attributed to the Fe-O group [2]. According to Maji et al. [36], the band at 1110 cm^{-1} corresponds to the crystalline Fe-O vibrations which is the characteristic of Fe_2O_3. This data corroborates the XRD results. The FTIR results also showed the disappearance of peaks 1020 cm^{-1}, 1730 cm^{-1}, and 2920 cm^{-1} after the formation of FeONP. This observation indicates the involvement of flavonoids/ organic acids/ carotenoids in the reduction process and synthesis of FeONP [25, 37].

3.1.4. Antioxidant Activity

The antioxidant activity of the green synthesized γ-Fe_2O_3 was evaluated using DPPH as a free radical model. Figure 4 shows the percentage of inhibition of DPPH. The results showed that the DPPH·scavenging activity increased from 10.91 to 33.03% when the quantity of γ-Fe_2O_3 increased from 0.0625 to 2 g. Therefore, γ-Fe_2O_3 showed remarkable antioxidant activity. That can be explained by the grapefruit peels' phytochemicals on the spherical surface of γ-Fe_2O_3 [25, 35].

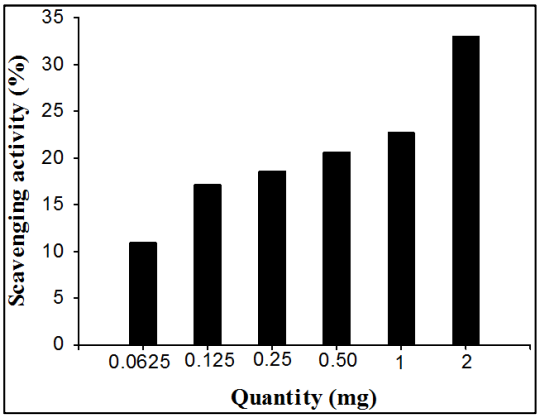

Figure 4. *Antioxidant activity of green synthesized Fe_2O_3 against DPPH.*

3.2. Adsorption Properties of Indigo Carmine in Aqueous Solution

3.2.1. Kinetic Adsorption Study

Figure 5 showed the effect of contact time on the adsorption of indigo carmine. The adsorption was fast during the first 5 min and increased slowly near the equilibrium. The vacant active sites' availability during the beginning adsorption experiment explained the rapid dye adsorption [14]. When the adsorption process increased, the indigo carmine molecules occupied the adsorption sites on γ-Fe_2O_3 [14, 38], thereby inducing slow adsorption. Indigo carmine adsorption equilibrium was reached at 60 min, with a maximum adsorption capacity of 1.90 mg/g. The experimental data were fitted by the nonlinear pseudo-first-order and nonlinear pseudo-second-order models (Figure 6). The results of kinetic model parameters are given in Table 1. The values of χ^2, and SSE obtained for the pseudo-second-order model were lower than those of the pseudo-first-order model. In addition, the R^2 value with pseudo-second-order (0.992) was higher than that of pseudo-first-order (0.865). Moreover, the results of the pseudo-second-model (Table 1) revealed that the maximum adsorption capacity obtained theoretically (Qe2 theo = 1.93 mg/g) is close to that obtained experimentally (Qe exp = 1.90 mg/g). Therefore, the pseudo-second-order was found to be the best model to fit indigo carmine adsorption. To understand the indigo carmine dye adsorption mechanism, the intraparticle diffusion model was applied. The results are shown in Figure 7 and Table 2. Figure 7 indicated that the plots did not pass through the origin, indicating that the indigo carmine adsorption process was not only governed by the pore diffusion process. Indigo carmine adsorption was biphasic, shown by two adsorption stages observed in Figure 7. The first part corresponds to the fast diffusion of indigo carmine from an aqueous solution to the γ-Fe_2O_3 outer surface [26, 39]. The intra-particle diffusion of indigo carmine into the interior of the γ-Fe_2O_3 pores is illustrated by the second part of the curves [26, 39]. In addition, the high value of R^2 (0.91) showed that the rate-limiting step was the intraparticle diffusion step [26, 39]. Therefore, the indigo carmine adsorption process is governed both by external surface adsorption and intra-particle diffusion.

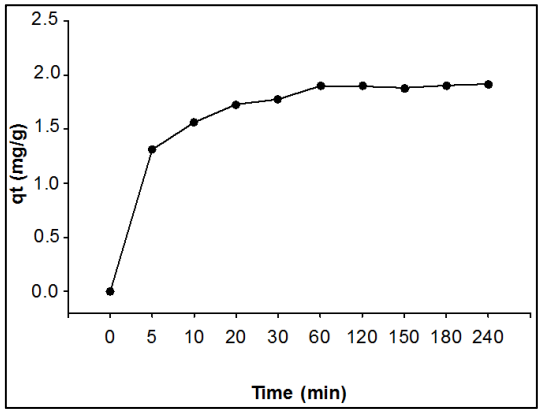

Figure 5. *Effect of contact time on adsorption capacities of indigo carmine.*

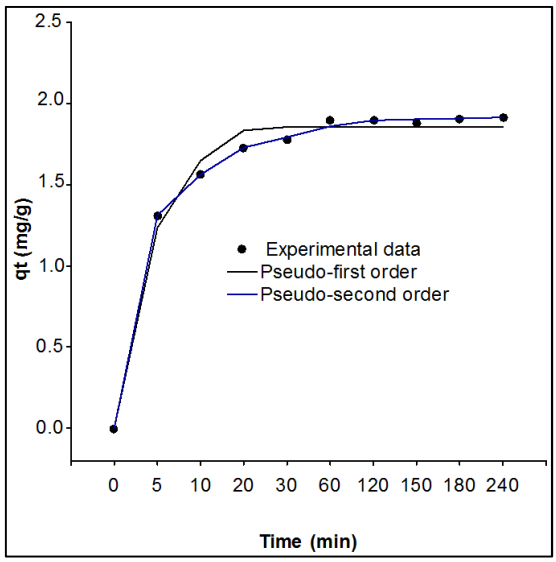

Figure 6. *Adsorption kinetics: nonlinear pseudo-first order model and nonlinear Pseudo-second order model for removal of indigo carmine.*

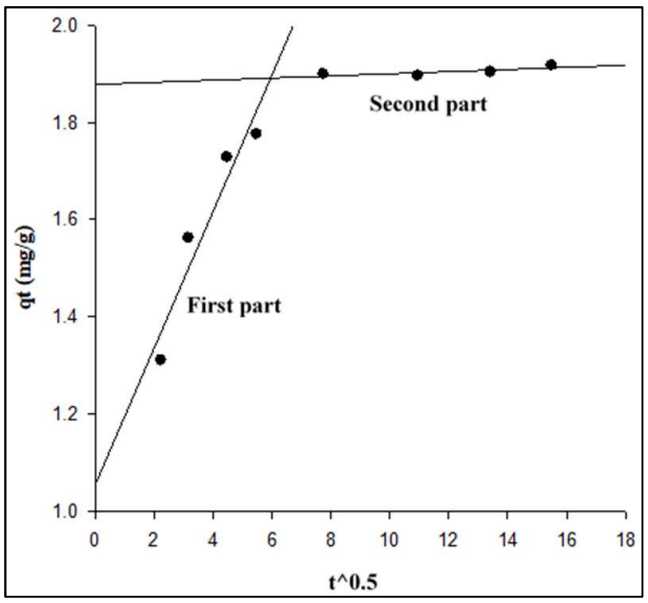

Figure 7. *Intra-particle diffusion model analysis.*

Table 1. *Parameters of pseudo-first-order, pseudo-second-order, Langmuir, Freundlich, and Sips models using nonlinear analysis.*

		Qe exp (mg/g): 1.90	
		Qe_1 (mg/g)	1.86
		k_1	0.218
	Pseudo first order	χ^2	0.024
		SSE	0.040
Kinetic		R^2	0.864
		Qe_2 (mg/g)	1.93
		k_2	0.217
	Pseudo second order	χ^2	0.0012
		SSE	0.0023
		R^2	0.992
		Qmax (mg/g)	7.83
		K_L	0.0079
	Langmuir	χ^2	0.025
		SSE	0.019
		R^2	0.9977
		K_F	0.1201
		n	1.344
Isotherm	Freudlich	χ^2	0.0314
		SSE	0.034
		R^2	0.9978
		K_S	0.0065
		m_S	0.859
	Sips	χ^2	0.016
		SSE	0.0115
		R^2	0.998

Table 2. *Parameters of intra-particle diffusion model.*

	First part	Second part
k_{id} ($mg.g^{-1}.min^{-1}$)	0.104	0.0022
C	1.056	1.877
R^2	0.91	0.63

3.2.2. Adsorption Capacity of Indigo Carmine in Aqueous Solution

The results of the influence of indigo carmine initial concentration on indigo carmine adsorption are shown in Figure 8a. The adsorption percentages of indigo carmine decreased with increasing initial concentrations due to the reduction of the active sites of γ-Fe_2O_3 [26]. The maximum adsorption percentage (96%) was obtained with an initial concentration value of 10 mg/L. The adsorption isotherm of indigo carmine onto γ-Fe_2O_3 is shown in Figure 8b. The adsorbed amounts of indigo carmine increase with increasing equilibrium concentration, indicating that the γ-Fe_2O_3 exhibited good adsorption capacity to indigo carmine [26]. The isotherm adsorption data were fitted by nonlinear forms of Langmuir, Freundlich, and Sips models (Figure 9 and Table 1). The results indicated that Langmuir's SSE and χ^2 values were smaller than those of the Freundlich model. In addition, Sips's SSE, χ^2, and K_S values were close to those of Langmuir. Therefore, indigo carmine adsorption isotherm was well described by the Langmuir model, thereby indicating a monolayer adsorption process. The results also revealed that indigo carmine adsorption on γ-Fe_2O_3 was favorable showing by R_L= 0.55. The maximum adsorption capacity (Qm) was 7.83 mg/g, indicating that γ-Fe_2O_3 could be a more promising indigo carmine adsorbent.

The maximum adsorption capacity (Qm = 7.83 mg/g) found in the present study was compared to data from the literature (Table 3). Data from this study was lower than those reported by El-Kammah et al. [14], Adel et al. [15], Odogu et al. [22], Tabi et al. [21], and Hevira et al. [40]. In contrast, data from Arenas et al. [41], de Olieira et al. [42], de Carvalho et al. [43], and Damasceno et al. [44] were higher than one obtained in the present study. Hence, γ-Fe_2O_3 synthesized with grapefruit peels has obvious advantages compared with some previously reported materials in Table 3.

Table 3. *Comparison of adsorption capacities of different adsorbents for indigo carmine removal.*

Adsorbents	Adsorption capacity Q (mg/g)	References
Moringa Oleifera Seed	60.2	[14]
$MgFe_2O_4$	46.08	[15]
Ricinodendron Heudelotti activated carbon	121.75	[22]
Palm Kernel Shell activated carbon	69.72	[21]
Terminalia Catappa	26.77	[40]
Risk husk ash	0.3-0.4	[41]
Brazil Nuts	1.09	[42]
Zeolites synthesized from coal fly ash	1.23	[43]
Superparamagnetic Fe_3O_4	6.12	[44]
γ-Fe_2O_3	7.83	Present study

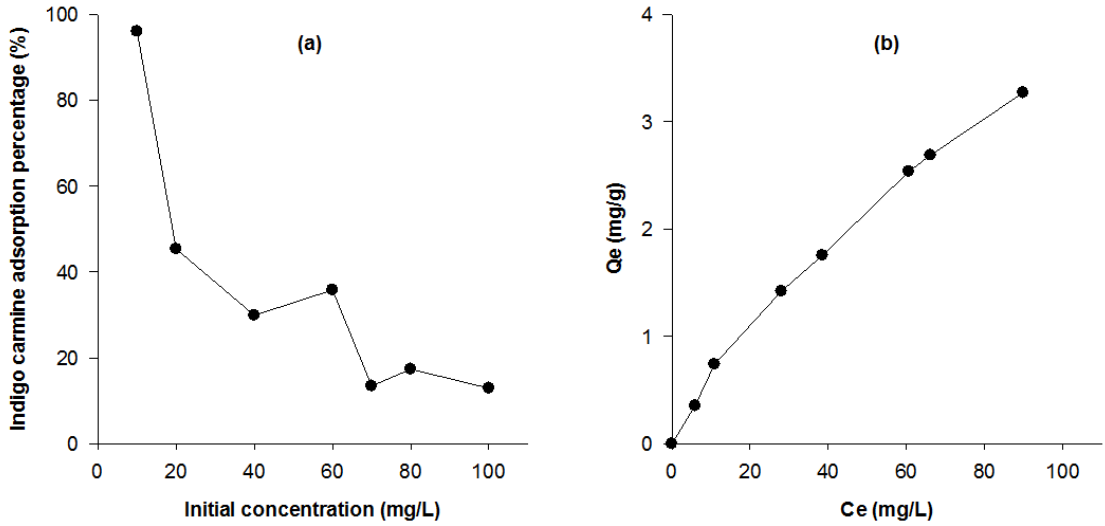

Figure 8. *Effect of initial concentration on indigo carmine removal (a), and adsorption isotherm of indigo carmine (b).*

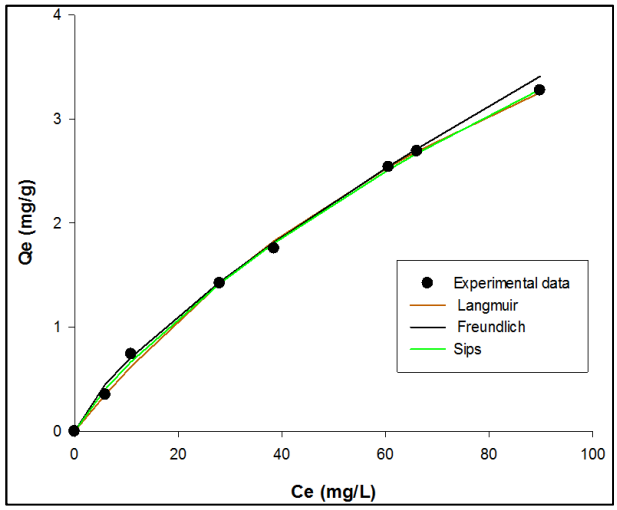

Figure 9. *Nonlinear Langmuir isotherm, nonlinear Freundlich isotherm, and nonlinear Sips isotherm for indigo carmine adsorption.*

3.2.3. Effect of pH on Indigo Carmine Adsorption

The influence of medium pH is shown in Figure 10b. The adsorption capacities of indigo carmine decreased when the solution pH increased. The maximum adsorption percentage 84.72% was obtained at pH 2.4. In this study, the value of the pH at the zero-point charge (pHpzc) is 6.4 (figure 10a). Below this value the surface of γ-Fe_2O_3 becomes positive. Therefore, there was an electrostatic attraction between the positively charged γ-Fe_2O_3 and indigo carmine which is an anionic dye, thereby explaining the higher adsorption capacity obtained at pH 2.4. On the contrary, when the solution pH is above pHpzc 6.4, the γ-Fe_2O_3 surface becomes negative. Therefore, the adsorption of indigo carmine is unfavorable due to electrostatic repulsion [14]. The higher adsorption capacities of indigo carmine at acidic pH were also reported by several authors [1, 15, 22, 45].

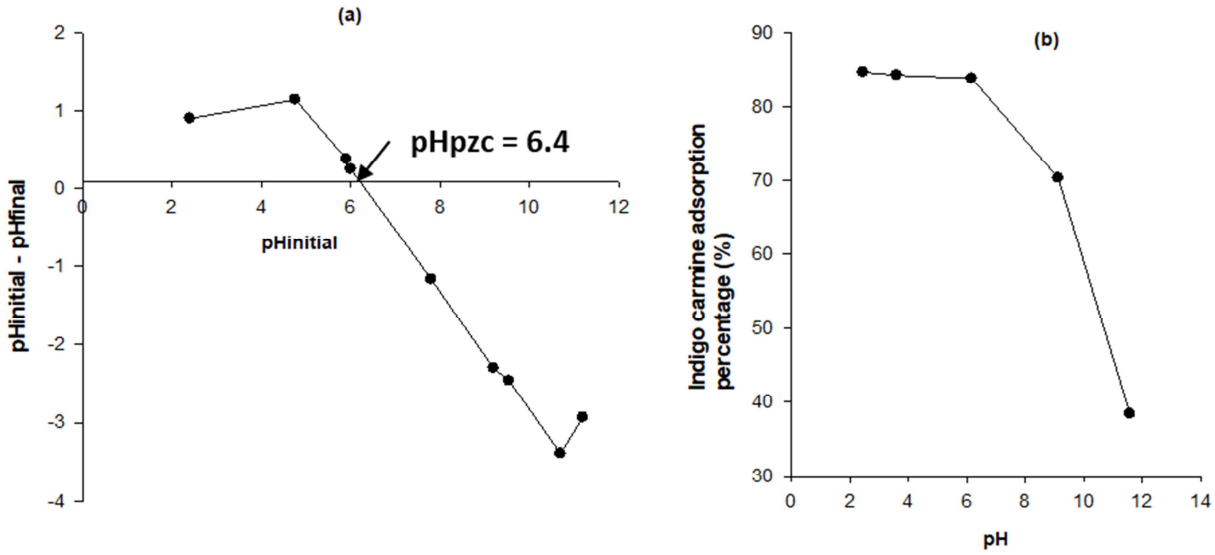

Figure 10. *pH at the point of zero charge (pHpzc) of Fe_2O_3 (a) and effect pH on adsorption capacities of indigo carmine (b).*

3.3. Removal of Indigo Carmine from Industrial Effluent

Table 4 gives the removal percentages of indigo carmine adsorbed from industrial effluent and the synthetic aqueous solution. The adsorption percentage of indigo carmine from the industrial effluent was 28.68%. The result obtained with industrial effluent was compared with a synthetic indigo carmine aqueous solution of 15.71 mg/L. It was found that the adsorption percentage found with industrial effluent (28.68%) was lower than that of the synthetic aqueous solution (78.67%). The decrease in indigo carmine removal from industrial effluent can be explained by the competition effects between indigo carmine and other pollutants present in the real effluent [26]. Thus, the green γ-Fe_2O_3 may be proposed to purify industrial effluents contaminated by indigo carmine.

Table 4. *Industrial effluents treatment.*

Sample	Before adsorption (mg/L)	After adsorption (mg/L)	Removal percentage (%)
Synthetic solution	15.71	3.35	78.67
Industrial effluent	13.70	9.77	28.68

4. Conclusion

In the present study, γ-Fe_2O_3 nanoparticles were successfully synthesized using grapefruit peel extract via the green method. The results of FTIR analysis showed that the synthesized γ-Fe_2O_3 surface is coated with grapefruit peel extract. The green γ-Fe_2O_3 nanoparticles were semi-spherical with an average crystallite size of 11.9 nm. The synthesized γ-Fe_2O_3 nanoparticles have been confirmed to show antioxidant activity against DPPH. The γ-Fe_2O_3 nanoparticle was used to remove indigo carmine from aqueous solution and from industrial effluent. In synthetic aqueous solution, the adsorption tests indicated that contact time, pH, and indigo carmine concentration affected indigo carmine removal. The maximum adsorption percentage 84.72% was obtained at pH 2.4. The kinetic study showed that the indigo carmine adsorption process was better described by the pseudo-second-order model, indicating that the chemisorption limits the adsorption process. The results also showed that the Langmuir model was the best to fit indigo carmine adsorption data, indicating a monolayer adsorption process. The maximum adsorption percentage in an aqueous solution was 96%. The investigation with industrial effluent indicated that the adsorption percentage of indigo carmine was 28.68%. With regard to the obtained results, the γ-Fe_2O_3 nanoparticles from grapefruit peel extract may be proposed to purify industrial effluents contaminated by indigo carmine.

References

[1] Ruíz-Baltazar, A. DJ., Reyes-López, S. Y., Mondragón-Sánchez, M. D. L., Robles-Cortés, A. I., Ramiro Pérez, R. (2019). Eco-friendly synthesis of Fe_3O_4 nanoparticles: Evaluation of their catalytic activity in methylene blue degradation by kinetic adsorption models. Results in Physics 12: 989–995. https://doi.org/10.1016/j.rinp.2018.12.037

[2] Abdullah, J. A. A., Eddine, L. S., Abderrhmane, B., Alonso-Gonzalez, M., Guerrero, A., Romero, A. (2020). Green synthesis and characterization of iron oxide nanoparticles by pheonix dactylifera leaf extract and evaluation of their antioxidant activity. Sustainable Chemistry and Pharmacy 17: 100280. https://doi.org/10.1016/j.scp.2020.100280

[3] Justin, C., Philip, S. A., Samro, A. V. (2017). Synthesis and characterization of superparamagnetic iron-oxide nanoparticles (SPIONs) and utilization of SPIONs in X-ray imaging. Applied Nanoscience 7: 463–475. https://doi.org/10.1007/s13204-017-0583-x

[4] Ali, H. R., Nassar, H. N., El-Gendy, N. S. (2017). Green synthesis of α-Fe_2O_3 using Citrus reticulum peels extract and water decontamination from different organic pollutants. Energy sources, part A: recovery, utilization, and environmental effects. https://doi.org/10.1080/15567036.2017.1336818

[5] Murugesan, K., Tareke, K., Gezehegn, M., Kebede, M., Yazie, A., Diyana, G. (2019) Rapid Development of Activated Carbon and ZnO Nanoparticles via Green Waste Conversion Using Avocado Fruit Peel Powder and its High Performance Efficiency in Aqueous Dye Removal Application. Journal of Inorganic and Organometallic Polymers and Materials 29: 1368–1374. https://doi.org/10.1007/s10904-019-01101-7

[6] Abdelghaffar, F. (2021). Biosorption of anionic dye using nanocomposite derived from chitosan and silver Nanoparticles synthesized via cellulosic banana peel bio-waste. Environmental Technology & Innovation 24 (2021) 101852. https://doi.org/10.1016/j.eti.2021.101852

[7] Kokila, T., Ramesh, P. S., Geetha, D. (2015). Biosynthesis of silver nanoparticles from Cavendish banana peel extract and its antibacterial and free radical scavenging assay: a novel biological approach. Applied Nanoscience 5: 911–920. https://doi.org/10.1007/s13204-0150401-2

[8] Wei, Y., Fang, Z., Zheng, L., Tan, L., Tsang, E. P. (2016). Green synthesis of Fe nanoparticles using Citrus maxima peels aqueous extracts. Materials Letters 185: 384–386. http://dx.doi.org/10.1016/j.matlet.2016.09.029

[9] Venkateswarlu, S., Yoon, M. (2015). Rapid removal of cadmium ions using greensynthesized Fe_3O_4 nanoparticles capped with diethyl-4-(4 amino-5-mercapto-4H-1,2,4-triazol-3-yl)phenyl phosphonate. RSC Advances, 5: 65444. http://dx.doi.org/10.1039/c5ra10628a.

[10] Agnihotri, S., Sillu, D., Sharma, G., Arya, R. K. (2018). Photocatalytic and antibacterial potential of silver nanoparticles derived from pineapple waste: process optimization and modeling kinetics for dye removal. Applied Nanoscience 8: 2077–2092. https://doi.org/10.1007/s13204-018-0883-9

[11] Abid, M. A., Abid, D. A., Aziz, W. J., Rashid, T. M. (2021). Iron oxide nanoparticles synthesized using garlic and onion peel extracts rapidly degrade methylene blue dye. Physica B 622: 413277. https://doi.org/10.1016/j.physb.2021.413277

[12] Patra, J. K., Kwon, Y., Baek, K. H. (2016). Green biosynthesis of gold nanoparticles by onion peel extract: Synthesis, characterization and biological activities. Advanced Powder Technology 27: 2204-2213. http://dx.doi.org/10.1016/j.apt.2016.08.005

[13] Santhosh, A., Theertha, V., Prakash, P., Chandran, S. S. (2021). From waste to a value added product: Green synthesis of silver nanoparticles from onion peels together with its diverse applications. Materials Today: Proceedings 46: 4460-4463 https://doi.org/10.1016/j.matpr.2020.09.680

[14] El-Kammah, M., Elkhatib, E., Gouveia, S., Cameselle, C., Aboukil, E. (2022). Enhanced removal of Indigo Carmine dye from textile effluent using green cost-efficient nanomaterial: Adsorption, kinetics, thermodynamics and mechanisms. Sustainable Chemistry and Pharmacy 29: 100753. https://doi.org/10.1016/j.scp.2022.100753

[15] Adel, M., Ahmed, M. A., Mohamed, A. A. (2021). Effective removal of indigo carmine dye from wastewaters by adsorption onto mesoporous magnesium ferrite nanoparticles. Environmental Nanotechnology, Monitoring & Management 16: 100550. https://doi.org/10.1016/j.enmm.2021.100550

[16] Pereira, P. C. G., Reimão, R. V., Pavesi, T., Saggioro, E. M., Moreira, J. C., Correia, F. V. (2017). Lethal and sub-lethal evaluation of Indigo Carmine dye and byproducts after TiO_2 photocatalysis in the immune system of Eisenia andrei earthworms. Ecotoxicology and Environmental Safety 143: 275–282. http://dx.doi.org/10.1016/j.ecoenv.2017.05.043

[17] Assemian, A. S., Kouassi, K. E., Drogui, P., Adouby, K., Boa, D. (2018). Removal of a Persistent Dye in Aqueous Solutions by Electrocoagulation Process: Modeling and Optimization Through. Water Air, and Soil Pollution 229: 184-197. https://doi.org/10.1007/s11270-018-3813-2

[18] Liu, X., Chen, Z., Du, W., Liu, P., Zhang, L., Shi, F. (2022). Treatment of wastewater containing methyl orange dye by fluidized three dimensional electrochemical oxidation process integrated with chemical oxidation and adsorption. Journal of Environmental Management 311: 114775. https://doi.org/10.1016/j.jenvman.2022.114775

[19] Rigueto, C. V. T., Alessandretti, I., Silva, D. H. D., Rosseto, M., Loss, R. A., Geraldi, C. A. Q. (2021) Agroindustrial Wastes of Banana Pseudo-stem as Adsorbent of Textile Dye: Characterization, Kinetic, and Equilibrium Studies. Chemistry Africa 4: 1069–1078. https://doi.org/10.1007/s42250-021-00263-7

[20] Sanni, S., Tchakala, I., Balogoun, C. K., Kodom, T., Bawa, M. L. (2022). Study of the Synthesis of Activated Carbon from Brewery Grains: Application to the Removal of the Cationic Dye Methylene Blue. American Journal of Physical Chemistry 11: 78-84.

[21] Tabi, G. A., Blaise, L. N. R., Daouda, K., Odogu, A. N., Victoire, A. A., Julius, N. N., Mbadcam, K. J (2022). Non-linear modelling of the adsorption of Indigo Carmine dye from wastewater onto characterized activated carbon/volcanic ash composite. Arabian Journal of Chemistry 15: 103515. https://doi.org/10.1016/j.arabjc.2021.103515

[22] Odogu, A. N., Daouda, K., Keilah, L. P., Tabi, G. A., Rene, L. N., Nsami, N. J., Mbadcam, K. J (2020). Effect of doping activated carbon based Ricinodendron Heudelotti shells with AgNPs on the adsorption of indigo carmine and its antibacterial properties. Arabian Journal of Chemistry 13: 5241–5253. https://doi.org/10.1016/j.arabjc.2020.03.002

[23] Gemeay, A. H., Elsharkawy, R. G., Aboelfetoh, E. F. (2018). Graphene Oxide/Polyaniline/Manganese Oxide Ternary Nanocomposites, Facile Synthesis, Characterization, and Application for Indigo Carmine Removal. Journal of Polymers and the Environment 26: 655–669. https://doi.org/10.1007/s10924-017-0947-z

[24] Fatombi, J. K, Esta A. Idohou, E. A., Osseni, S. A., Agani, I., Neumeyer, D., Verelst, M., Mauricot, R., Aminou, T. (2019). Adsorption of Indigo Carmine from Aqueous Solution by Chitosan and Chitosan/Activated Carbon Composite: Kinetics, Isotherms and Thermodynamics Studies. Fibers and Polymers 20: https://doi.org/1820-1832.10.1007/s12221-019-1107-y

[25] Kumar, B., Smita, K., Galeas, S., Sharma, V., Guerrero, V. H., Debut, A., Cumbal, L. (2020). Characterization and application of biosynthesized iron oxide nanoparticles using Citrus paradisi peel: A sustainable approach. Inorganic Chemistry Communications 119: 108116. https://doi.org/10.1016/j.inoche.2020.108116

[26] Kouassi, N. L. B., N'goran, K. P. D. A., Blonde, L. D., Diabate, D., Albert, T. (2022). Simultaneous Removal of Copper and Lead from Industrial Effluents Using Corn Cob Activated Carbon. Chemistry Africa. https://doi.org/10.1007/s42250-022-00432-2

[27] Chen, X., Mao, S. S. (2007). Titanium Dioxide Nanomaterials: Synthesis, Properties, Modifications, and Applications. Chemical Reviews 107: 2891-2959. https://doi.org/10.1021/cr0500535

[28] Lagergren, S. (1898). About the theory of so-called adsorption of soluble substances. Kungliga Svenska Vetensk Handl 24: 1–39.

[29] Ho, Y. S., McKay, G. (1999). Pseudo-second order model for sorption processes. Process Biochemistry 34: 451–465. https://doi.org/10.1016/S0032-9592(98)00112-5

[30] Weber, W. J., Morris, J. C. (1963). Kinetics of Adsorption on Carbon from Solution. J Sanit Eng Div Am Soc Civ Eng 89: 31–60. https://doi.org/10.1061/JSEDAI.0000430

[31] Langmuir, I. (1906). The adsorption of gases on plane surfaces of glass mica and platinum. Journal of the American Chemical Society 40: 1361–1403. https://doi.org/10.1021/ja02242a004

[32] Freundlich HMF (1906) Über die adsorption in lösungen. Z PhysChem-Frankfurt 57A: 385-470. https://doi.org/10.1515/zpch-1907-5723

[33] Saruchi, Kumar, V. (2019). Adsorption kinetics and isotherms for the removal of rhodamine B dye and Pb^{+2} ions from aqueous solutions by a hybrid ion-exchanger. Arabian Journal of Chemistry 12: 316–329. http://dx.doi.org/10.1016/j.arabjc.2016.11.009

[34] Bhuiyan, M. S. H., Miah, M. Y. M., Paul, S. C., Aka, T. D., Saha, O., Rahaman, M. M., Sharif, M. J. I., Habiba, O., Ashaduzzaman, M. (2020) Green synthesis of iron oxide nanoparticle using Carica papaya leaf extract: application for photocatalytic degradation of remazol yellow RR dye and antibacterial activity. Heliyon 6: e04603. https://doi.org/10.1016/j.heliyon.2020.e04603

[35] Kumar, B., Smita, K., Cumbal, L., Debut, A., Galeas, S., Guerrero, V. H. (2016). Phytosynthesis and photocatalytic activity of magnetite (Fe_3O_4) nanoparticles using the Andean blackberry leaf. Materials Chemistry and Physics 179: 310-315. http://dx.doi.org/10.1016/j.matchemphys.2016.05.045

[36] Maji, S. K, Mukherjee, N., Mondal, A., Adhikary, B. (2012). Synthesis, characterization and photocatalytic activity of α-Fe_2O_3 nanoparticles. Polyhedron 33: 145–149. http://dx.doi.org/10.1016/j.poly.2011.11.017.

[37] Kumar, B., Smita, K., Cumbal, L., Debut, A. (2014). Biogenic synthesis of iron oxide nanoparticles for 2-arylbenzimidazole fabrication. Journal of Saudi Chemical Society: 18, 364–369. http://dx.doi.org/10.1016/j.jscs.2014.01.003

[38] Ferreira, R. M., de Oliveira, N. M., Lima, L. L. S., Campista, A. L. D. M., Stapelfeldt, D. M. A. (2019). Adsorption of indigo carmine on Pistia stratiotes dry biomass chemically modified. Environmental Science and Pollution Research 26: 28614–28621. https://doi.org/10.1007/s11356-018-3752-x

[39] Gholamiyan, S., Hamzehloo, M., Farrokhnia, A. (2020). RSM optimized adsorptive removal of erythromycin using magnetic activated carbon: adsorption isotherm, kinetic modeling and thermodynamic studies. Sustainable Chemistry and Pharmacy 17: 100309–100311. https://doi.org/10.1016/j.scp.2020.100309

[40] Hevira, L., Zilfa, Rahmayenid, Ighalo, J. O., Zein, R. (2020). Biosorption of indigo carmine from aqueous solution by Terminalia Catappa shell. Journal of Environmental Chemical Engineering 8: 104290. https://doi.org/10.1016/j.jece.2020.104290

[41] Arenas, C. N., Vasco, A., Betancur, M., Martínez, J. D. (2017). Removal of indigo carmine (IC) from aqueous solution by adsorption through abrasive spherical materials made of rice husk ash (RHA). Process Safety and Environmental Protection 106: 224-238. https://doi.org/10.1016/j.psep.2017.01.013

[42] de Oliveira, B. S. M., Andrade, H. M. C., Soares, L. F., de Azevedo, R. P. (2010). Brazil nut shells as a new biosorbent to remove methylene blue and indigo carmine from aqueous solutions. Journal of Hazardous Material 174: 84–92. https://doi.org/10.1016/j.jhazmat.2009.09.020

[43] de Carvalho, T., Fungaro, D., Magdalena, C., Cunico, P. (2011). Adsorption of indigo carmine from aqueous solution using coal fly ash and zeolite from fly ash. Journal of Radioanalytical and Nuclear Chemistry 289: 617–626. https://doi.org/10.1007/s10967-011-1125-8

[44] Damasceno, B. S., Silva, A. F. D., Araújo, A. C. Y. D. (2020). Dye adsorption onto magnetic and superparamagnetic Fe_3O_4 nanoparticles: A detailed comparative study. Journal of Environmental Chemical Engineering 8: 103994. https://doi.org/10.1016/j.jece.2020.103994

[45] Harrache, Z., Abbas, M., Aksil, T., Trari, M. (2019). Thermodynamic and kinetics studies on adsorption of Indigo Carmine from aqueous solution by activated carbon. Microchemical Journal 144: 180-189. https://doi.org/10.1016/j.microc.2018.09.004